

Appendix A: Model details and supporting demographic analyses for On using Integral Projection Models to generate demographically driven predictions of species distributions: development and validation using sparse data

Cory Merow, Andrew Latimer, Adam Wilson, Sean McMahon, Tony Rebelo, John Silander

April 2, 2014

Contents

1	Data	2
1.1	Environmental Data	2
1.2	Occurrence Data	2
2	Vital Rate Regressions	2
3	Growth	3
4	Survival	5
5	Fecundity	9
5.1	Seedheads per individual	9
5.2	Offspring size	11
5.3	Flowering Probability	13
5.4	Seeds/Seedhead	13
5.5	Recruitment	13
6	Kernels	15
7	Analyses	17
8	Uncertainty	18
9	Sensitivity/Elasticity	22
10	References	30

1 Data

In this section, we describe decisions made while handling various aspects of the data.

1.1 Environmental Data

Some explanation of the environmental predictors we used is warranted. Soil moisture days (SMD) are counted as the number of days in summer when modeled soil moisture exceeds a threshold value (Schulze 2007). The threshold was based on crop plants and so is not directly parameterized for the much more drought-tolerant fynbos shrubs, but the number of days with freely available soil moisture nonetheless serves as a useful relative index of seasonal soil moisture availability for plants generally. Edaphic factors were defined for each 1 x 1 arcminute grid cell as the percentage of the cell that contains a particular soil class (e.g. high fertility soil) (Latimer et al. 2006). While these do not directly quantify the edaphic attributes experienced by an individual or population (e.g. they do not define the average soil pH), they can be interpreted as the probability that an individual occurs on a particular soil type. Summer SMD was highly correlated with mean annual precipitation (0.86), however we chose to use summer SMD because its distribution across the region was somewhat less skewed than mean annual precipitation and had lower DIC values in all regressions except for the survival models (discussed below). Also, the Cape Floristic Region was masked to exclude areas that have been converted to agriculture, urban and suburban landscapes or dominated by dense alien stands (e.g. alien *Acacia* or *Hakea* spp). This layer was generated using LandSat images with extensive ground-truthing to produce a binary vector layer (Richard Cowling, personal communication).

1.2 Occurrence Data

The Protea Atlas database derives from a citizen science initiative to record occurrence and ordinal abundance data (0, [1-10], (10-100], (100-1000], (1000,Inf) individuals) for all 283 Proteaceae species throughout the Cape Floristic Region and contains 250,000 records over 90,000 km² (Rebelo 2002). The atlas data were first summarized to include the maximum observed abundance of *P. repens* within each grid cell (which could be zero). This summary resulted in many potentially false absences, because the surveys did not constitute exhaustive samples of the complete grid cell and the data are likely to have inflated observations of other more rare species that atlasers were more motivated to survey. Thus there are many grid cells within the core range of *P. repens* that have no reported presences but cannot be considered true absences. To remove this bias, we subjected sampled cells without *P. repens* observations to an additional spatial filter to remove cells reporting absences where a nearby cell reported a presence. The filter was implemented as a 5x5 cell moving window, where any absence was removed if a presence was observed within the 5x5 cell window. This has the effect of removing 1,235 ‘absences’ in cells that are mostly interspersed within the core range of the species. The remaining 2338 absence locations are mostly on the range fringes and therefore can provide a sound test of whether our DDDMs adequately differentiate suitable habitat from clearly unsuitable habitat (Figure 3, main text).

2 Vital Rate Regressions

To generate each vital rate regression model, all six candidate environmental predictors were first included in univariate (generalized) linear models that included size as a predictor to determine whether they had any explanatory power for the each vital rate. Quadratic transformations of the predictors were important to allow for the possibility of unimodal responses, which are expected if the species entire range is included in the model (e.g. some locations are either too wet or too dry, with preferable locations in between, cf. Austin 2007). If either linear or quadratic transformations were significant ($p < 0.05$), both transformations were included in the full model as candidates. This procedure reduced the size of the model space searched (compared to including all transformations of all predictors) during stepwise selection by removing the least informative covariates. The full model was then subjected to backward stepwise DIC (Deviance Information Criterion; Spiegelhalter et al. 2002) selection, where reduced models were accepted if their associated DIC was no worse than 3 units larger than that of the full model. Environmental predictors were standardized. Note that summer soil moisture days were selected instead of mean annual precipitation in some models where the DIC was comparable (within 3 units) due to high precipitation in some regions with no demographic data (resulting in the need for extreme

extrapolation; see Fig. 4d, main text). See the results/discussion section in the main text which we discuss issues of extrapolation in environmental space.

3 Growth

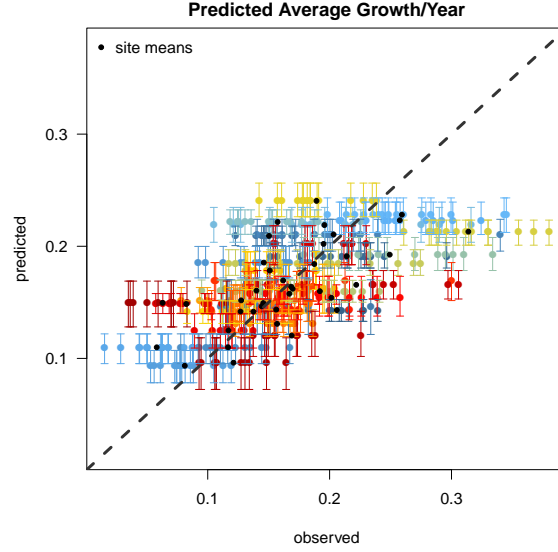


Figure A1: The predictions are shown for the 38 plots where growth was measured. Colors correspond to different plots. Dashed line indicates the 1:1 line. Although plot means (black dots) are well predicted, a large amount of variation exists among individuals. We used length of the central branch as a measure of size; actual plant height is approximately $0.86 \times$ this length, based on plants where both central branch length and height were measured.

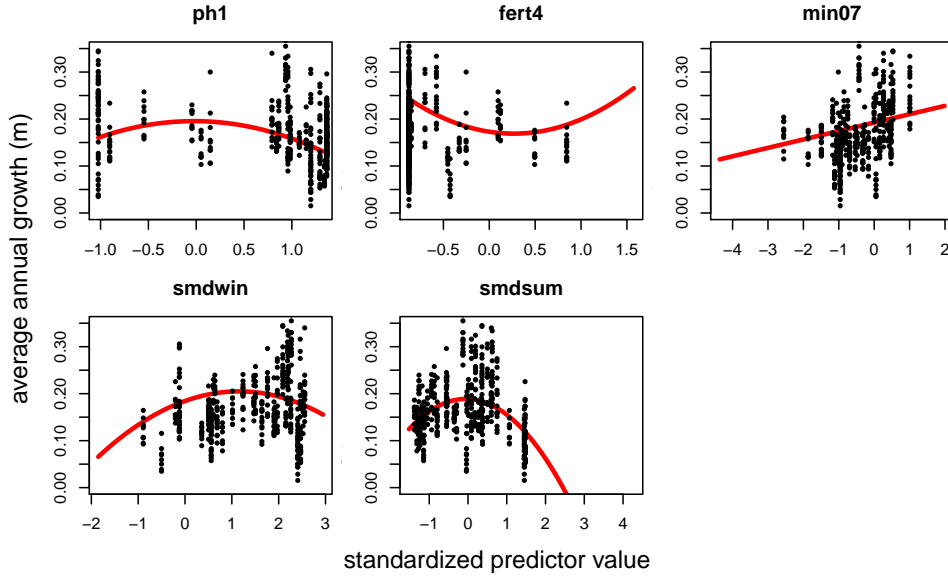


Figure A2: Partial dependence plots for candidate predictors in the growth model. All predictors have been standardized and the range on the horizontal axis reflects the range of each predictor across the entire region. For each plot, all predictors besides the focal predictor were held at their mean values across the region (Fig. 1 in the main text). Note that the concave upward response to high soil fertility (% fert4) is somewhat difficult to interpret. We interpret this as a declining response to soil fertility because the increasing relationship for values greater than 0.5 occurs in very few cells in the region (Fig. 1, Main text). Furthermore, there is very low sensitivity and elasticity with respect to λ in these rare high fertility locations, so the portion of the curve above 0.5 has very little impact on predictions.

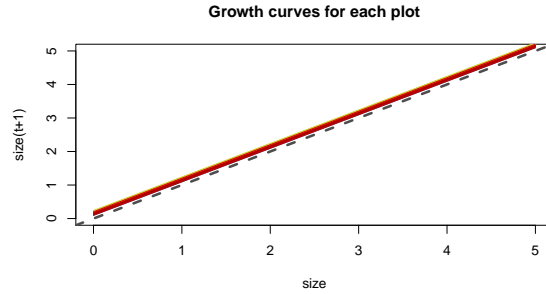


Figure A3: Growth trajectory. The predictions are shown for the 38 plots where growth was measured. Colors correspond to different plots. Note that zooming in is necessary to see the different curves, which differ only in their intercept. As a simplification, due to the limitations of our data, we modeled average interannual growth increment (the intercept). The average increment (averaged over the individuals' lifespan) was not modeled with size dependence, hence $\text{size}[t+1] = \text{size}[t] + \text{modeled growth increment}$. Although the size dependence of growth is likely important for many species, ignoring size dependence in most *Proteas* not an unreasonable assumption because they typically add one segment to each branch each year. Infrequently, *P. repens* adds multiple segments in a single year, which prevented us from assigning segments to years. That is, for a 10 year old individual with 11 segments, it is unclear which year had two segments.

4 Survival

The survival model is informed by two data sets and the output of both the growth and fecundity models. The first data set consists of transects in which the number of living and dead adults were recorded and the second consisted of parent-seedling ratios. Of course, it would be preferable to have sequential observations of individuals to directly observe survival, but in the absence of such data, we illustrate a work-around. The underlying survival model is a logistic model for a survival probability as a function of individual size and environmental covariates (mean annual precipitation and minimum winter temperature).

To estimate size dependent survival from both data sets, we must infer the size of individuals based on the growth model and the time since fire (unfortunately, size was not measured for these individuals). This is simplest for the transect data on adult survival. From the data, we know the time since fire and the number of live and dead adults for a sample from the population. Using the growth model, we estimated the size of the individuals by summing the average annual growth for the number of years since fire. This enables us to use size as a predictor for the logistic regression. The model can be implemented with the following algorithm for the adult mortality transect data.

1. Sample growth model posterior.
2. Predict individual size based on site age for the survival transect data.
3. Specify uninformative prior on survival model parameters.
4. Fit survival model as a function of size and environment.
5. Record posterior distribution of parameters.

To infer survival probabilities for seedlings and juvenile plants we used parent-seedling ratios obtained from a single visit to a site. The number of seedlings from the year before survey was unknown and thus was predicted. To do this, we began by predicting the size of the parent plants using the fitted growth regressions and the (known) age of the plot when it burned. Using predicted size, we then estimated their production of seeds using the fitted regressions for the number of seedheads per individual and the number of seeds per seedhead (see below). We used the recruitment model described below to predict the number of recruits from these seeds. We then imputed the growth of the seedlings until the year prior to surveying. Then, we could model survival probability by relating the number of observed live seedlings to imputed live seedlings in the previous year using logistic regression.

Due to the relatively small sample size of the survival data sets (16 transects for juvenile survival and 127 transects in only 43 unique grid cells), we did little variable selection for these models. We expected that both temperature and precipitation are related to mortality, especially of seedlings (e.g. Latimer et al. 2009), so we included one temperature variable and one relatively orthogonal precipitation variable in each model. After fitting the models, we created maps of the resulting predicted survival rates across the region to check whether they produced biologically implausible patterns. This caused us to reject, for the adult model, the number of summer soil moisture days (SMDSUM) in favor of mean annual precipitation.

As plant growth is gradual and continuous, we decided to smooth the transition from seedling to adult survival rates rather than using a step function that would be implied by the use of the two separate models. We set the sizes of this transition based on the mean expected sizes between 1-4 years, determined from the intercept of the growth model (i.e. between the sizes of 0.182 cm and 0.728 cm; vertical dashed lines in Fig. A7). We smoothed the survival rate transitions linearly from the seedling to the (generally much higher) adult survival rate.

The resulting shapes of survival curve are not entirely surprising (Fig. A7), and are qualitatively similar to a logistic function of size with a positive size coefficient and a negative size² coefficient. Initially, seedling survival is predicted to be low, followed by an abrupt increase in survival. This increase corresponds well with *P. repens*' life history; once established, a taproot typically hits the water table by the third year, after which mortality is extremely low. In most locations (suitably warm and moist), adult mortality is extremely low. However, in marginal habitats adult mortality may be somewhat higher (e.g. pink/purple curves in Fig. A7, corresponding to cold, dry locations bordering the Great Karoo Desert).

In spite of the apparently reasonable predictions of the survival model, there is reason for cautious interpretation. Fig. A4 suggests that the strong decrease of survivorship for large plants is driven by a few sites with low survival for which the imputed size is very large. While senescence certainly exists in *Protea repens*, it is unclear

whether 4 m tall plants really have an annual survival rate that is as low as suggested by these data. Further, the survival model contains substantial uncertainty: size was not measured directly in censuses quantifying adult survivorship but was inferred as average predicted size at a location given the time since fire, which was in turn predicted from the growth model. Since the size of surviving and dead plants is not known, it is conceivable that those individuals that died were smaller than the average in their population. It could even be that the low survival of large plants shown in Fig. A4 was actually due to the low survival on young inter-fire recruits on old sites. (Interfire recruits are rare and primarily occur at old sites.) In both cases, the survival model would underestimate survival of large plants. Hence, it is possible that the survival models underestimate survival of large plants. This has implications for the elasticity analyses described below and in figure 6 in the main text; the elasticity to adult survival may be lower than our model predicts. Rather than view these uncertainties in our model as a weakness, we interpret them as important insights for future study. Although prevailing expert knowledge suggests that adult survival may be higher than our model predicts, we have made the first attempt to describe range-wide survival patterns and hence have quantitative evidence to challenge these expectations. Our somewhat surprising results can help to generate new hypotheses about constraints on survival and target future data collection, specifically in large adult survival along moisture gradients.

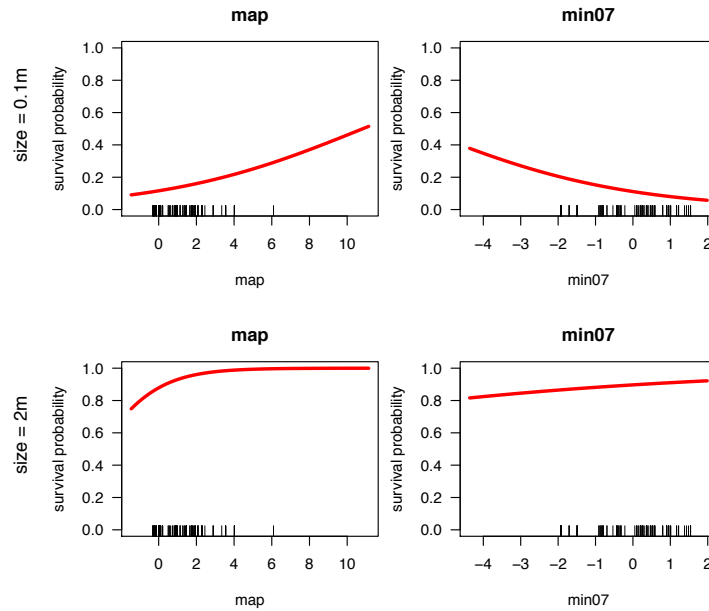


Figure A4: Predicted survival probability for 0.1m (top row) and 2.0m (bottom row) individuals as a function of mean annual precipitation (map) and minimum winter temperature (min07). All predictors have been standardized and the range on the horizontal axis reflects the range of each predictor across the entire region (Fig. 1 in the main text). For each plot, all predictors besides the focal predictor were held at their mean values across the region.

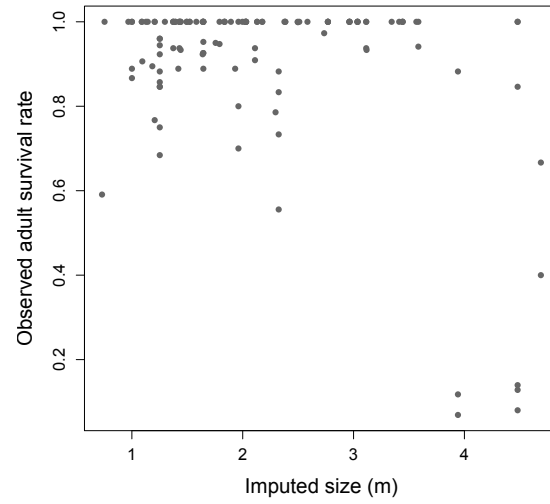


Figure A5: Survival 'data' based on adult size imputed from the growth model and time since fire (imputed size=offspring size + ($\#$ years since fire - 1)*average annual growth). Note the strong decline in survival probability for larger plants/older populations.

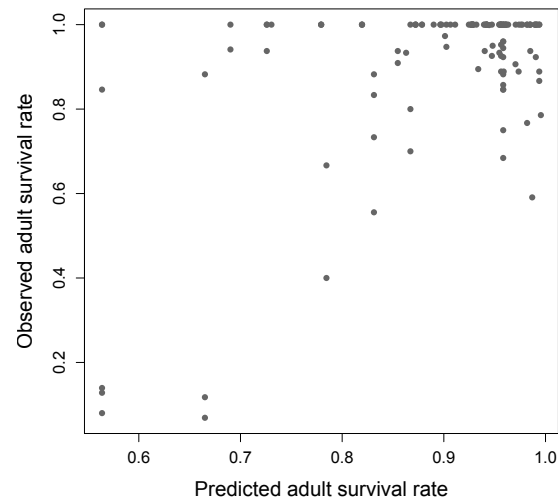


Figure A6: Survival predictions.

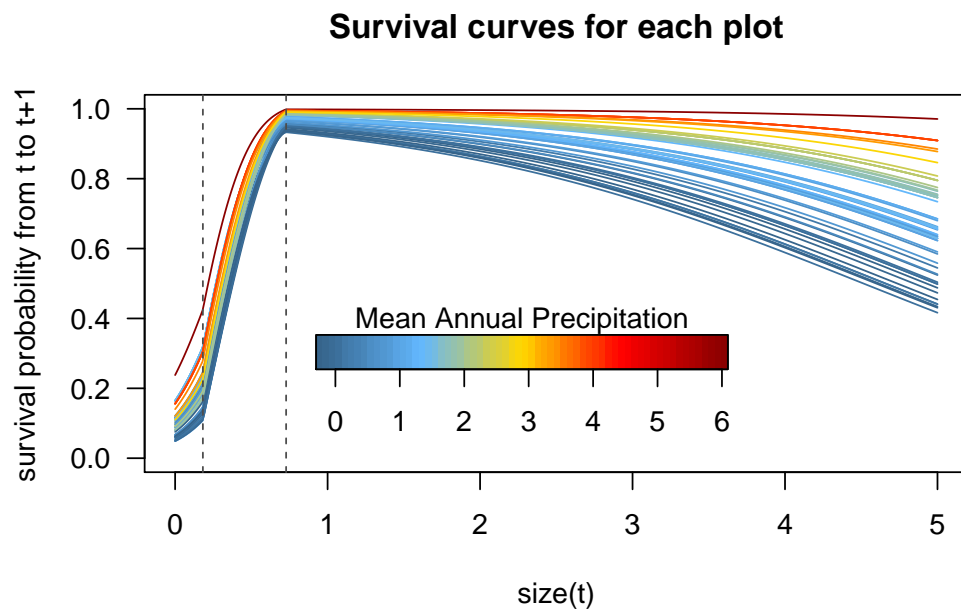


Figure A7: Size dependence of survival, calculated at the 43 unique grid cells where survival was measured. Vertical dashed lines indicate the bounds of smoothing between the seedling and adult survival models. These bounds were chose to reflect the average size of 1- (lower) to 4-year olds (upper).

5 Fecundity

5.1 Seedheads per individual

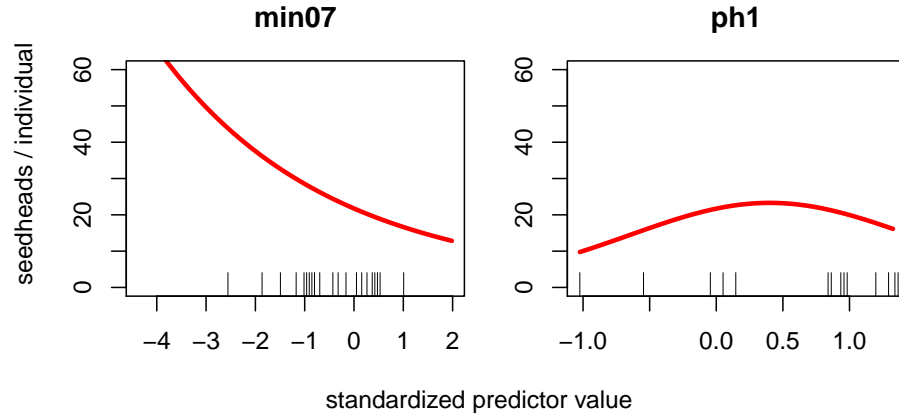


Figure A8: Partial dependence plots for predictors in the seedhead model. All predictors have been standardized and the range on the horizontal axis reflects the range of each predictor across the entire region. For each plot, all predictors besides the focal predictor were held at their mean values across the region (Fig. 1 in the main text). Rug plot indicates the location of data points used for fitting. More data are clearly needed at the lower end of the minimum July temperature (min07) gradient. The sharp increase in seedhead production with colder temperatures may be unrealistic, and leads to the higher predicted values of along the northern edge of the Cape Floristic Region in the east, bordering the Great Karoo.

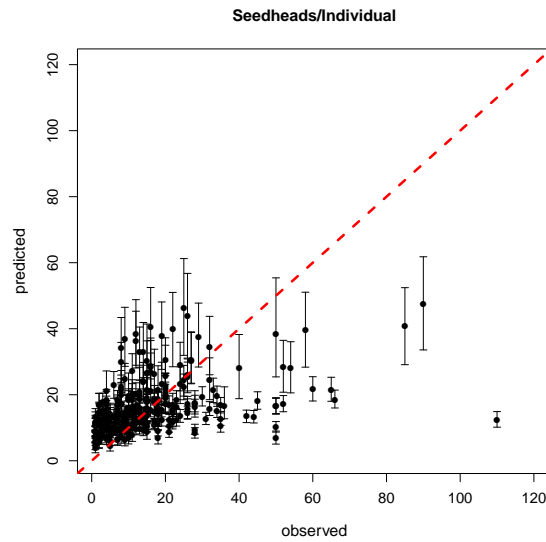


Figure A9: Predicted number of seedheads plotted versus observations, with credible intervals.

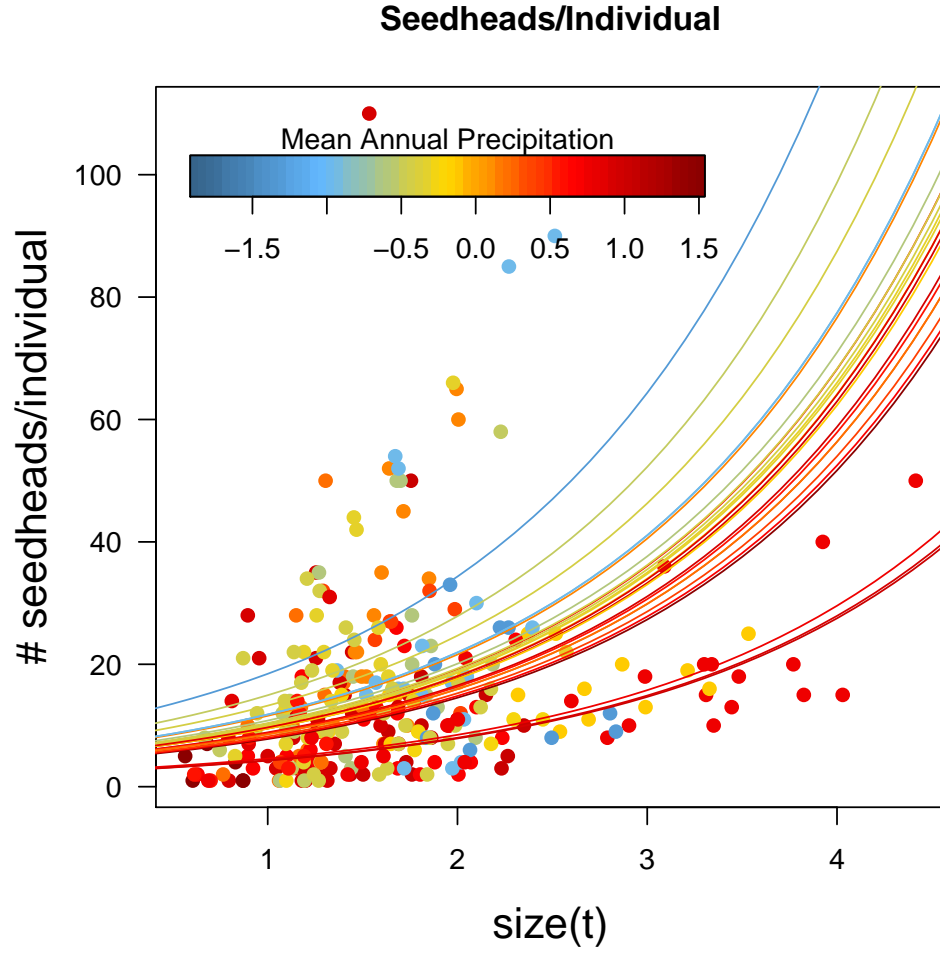


Figure A10: Predicted size dependence of seedhead production, with data points used for fitting. Different colors correspond to different sampling locations. Mean annual precipitation has been standardized across the entire region. All other predictors were held at their mean values across the region (Fig. 1 in the main text).

5.2 Offspring size

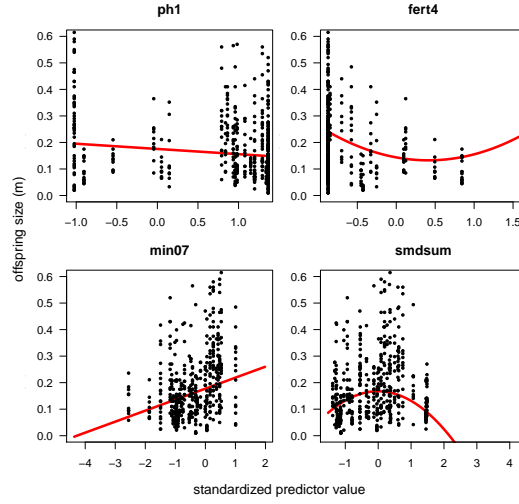


Figure A11: Partial dependence plots for candidate predictors in the offspring size model. All predictors have been standardized and the range on the horizontal axis reflects the range of each predictor across the entire region. For each plot, all predictors besides the focal predictor were held at their mean values across the region (Fig. 1 in the main text). Offspring size was estimated from the first internode length along the central branch segment that was used to as a measure of size. This approximation for offspring size was necessary because it was not measured at sites where parent-seedling ratios were collected. Note that the concave upward response to high soil fertility (% fert4) is somewhat difficult to interpret (this is also observed in the growth model in Fig. A2). We interpret this as a declining response to soil fertility because the increasing relationship for values greater than 0.5 occurs in very few cells in the region (Fig. 1, Main text). Furthermore, there is very low sensitivity and elasticity with respect to λ in these rare high fertility locations, so the portion of the curve above 0.5 has very little impact on predictions.

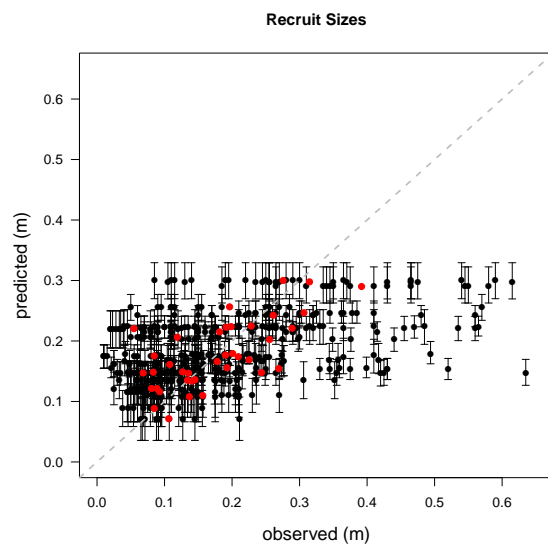


Figure A12: Black circles show predictions for individuals; red circles show the mean site level predictions. The pattern in site level differences is reasonably well predicted, however much variation remains among individuals within each site.

5.3 Flowering Probability

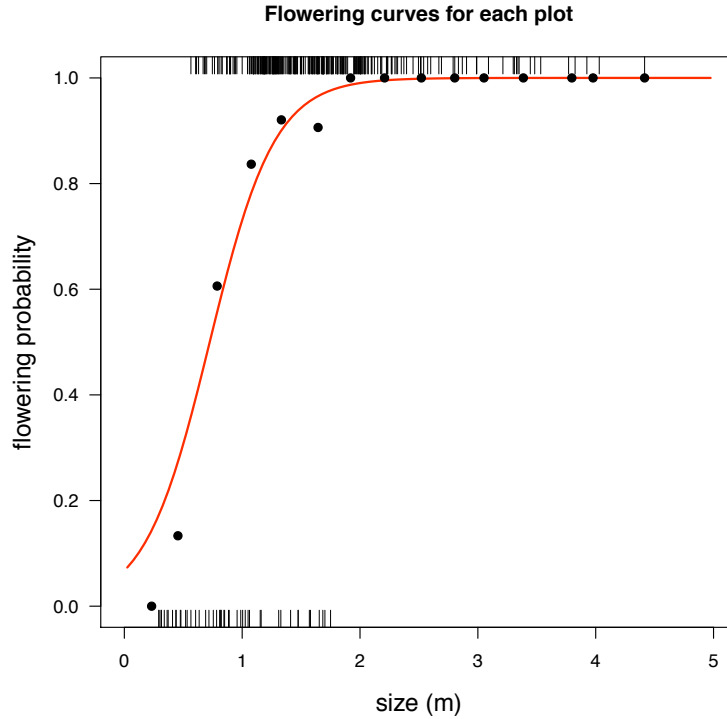


Figure A13: The rug plots show the locations of the data which were used to fit the model, while the black circles show proportion of individuals flowering within binned size classes (for easier visualization).

5.4 Seeds/Seedhead

This regression was performed only on 'new' seedheads (other designations were 'medium' and 'old') that had more than 10 seeds. These cutoffs reflect the observation is that there are many sources of seed loss, none of which we model explicitly. These seed predictions are used to estimate recruitment below. By only using the total number of new seedheads that don't appear to have suffered seed predation, etc., we included all sources of seed loss in to a single 'black box' reflecting the transition from seed production to recruitment.

5.5 Recruitment

We have a single estimate of recruitment probability common to the whole region. In analogy with the seedling survival model above, this proceeds by:

1. Sample growth model posterior.
2. Predict average inter-annual growth at 1 year old sites.
3. Predict parent size based on site age at the time of burn.
4. Sample seedhead number model posterior.
5. Predict the number of seeds per individual based on parent size.
6. Predict the total number of seeds produced along the transect from the total number of parents.
7. Predict the recruitment probability as the number of observed seedlings divided by the number of predicted seeds.

8. Record the predicted recruitment probability.
9. Return to step 1 (e.g. 1000 times).

This results in the following posterior density for recruitment probability:

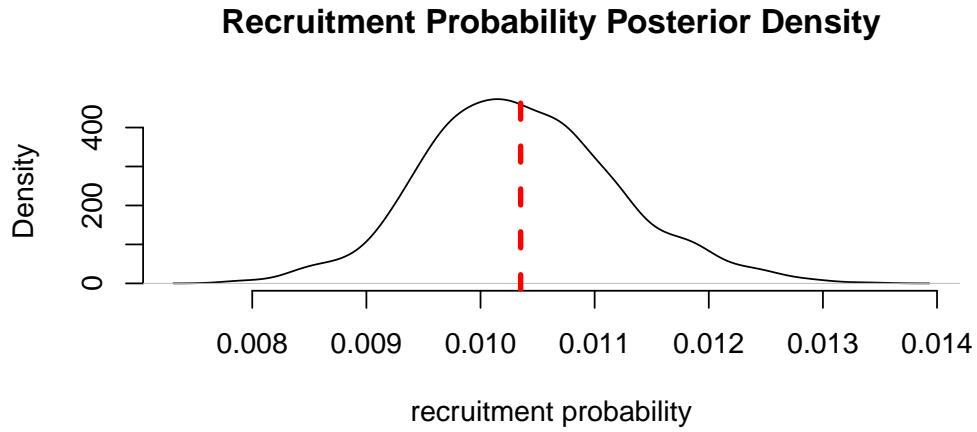


Figure A14: Posterior density of recruitment probability, including all sources of uncertainty in imputed parent size and seed production.

6 Kernels

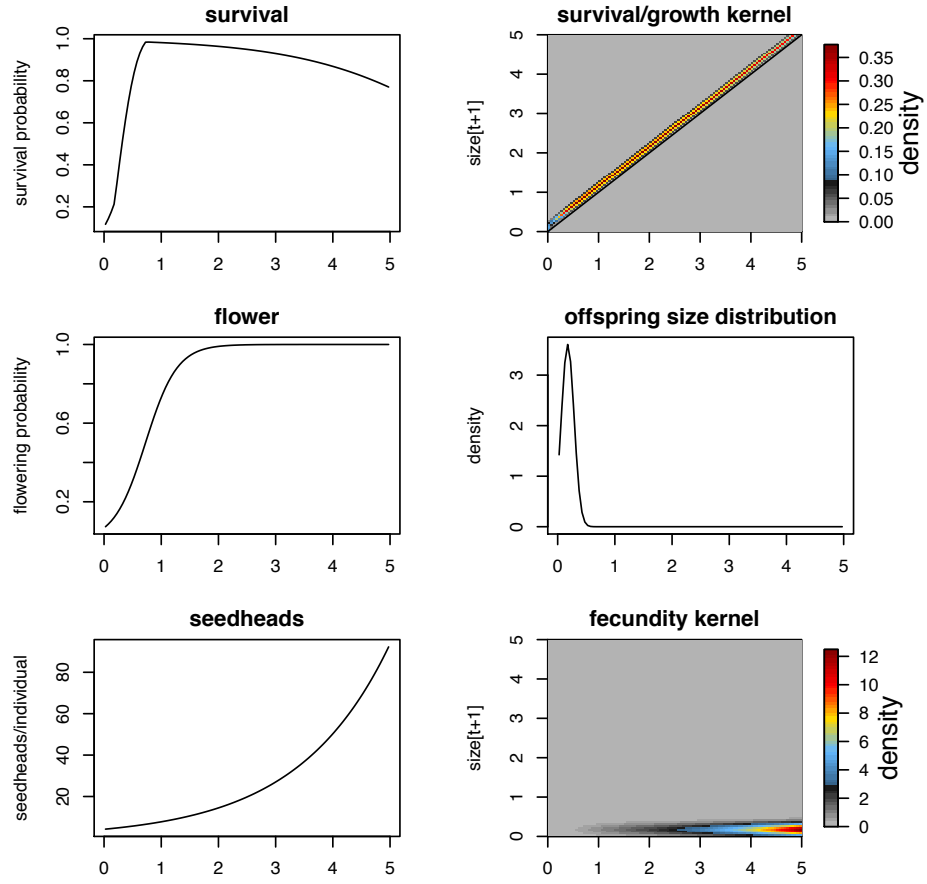


Figure A15: An example of the regressions and the kernel for a location with positive population growth ($\lambda=1.14$).

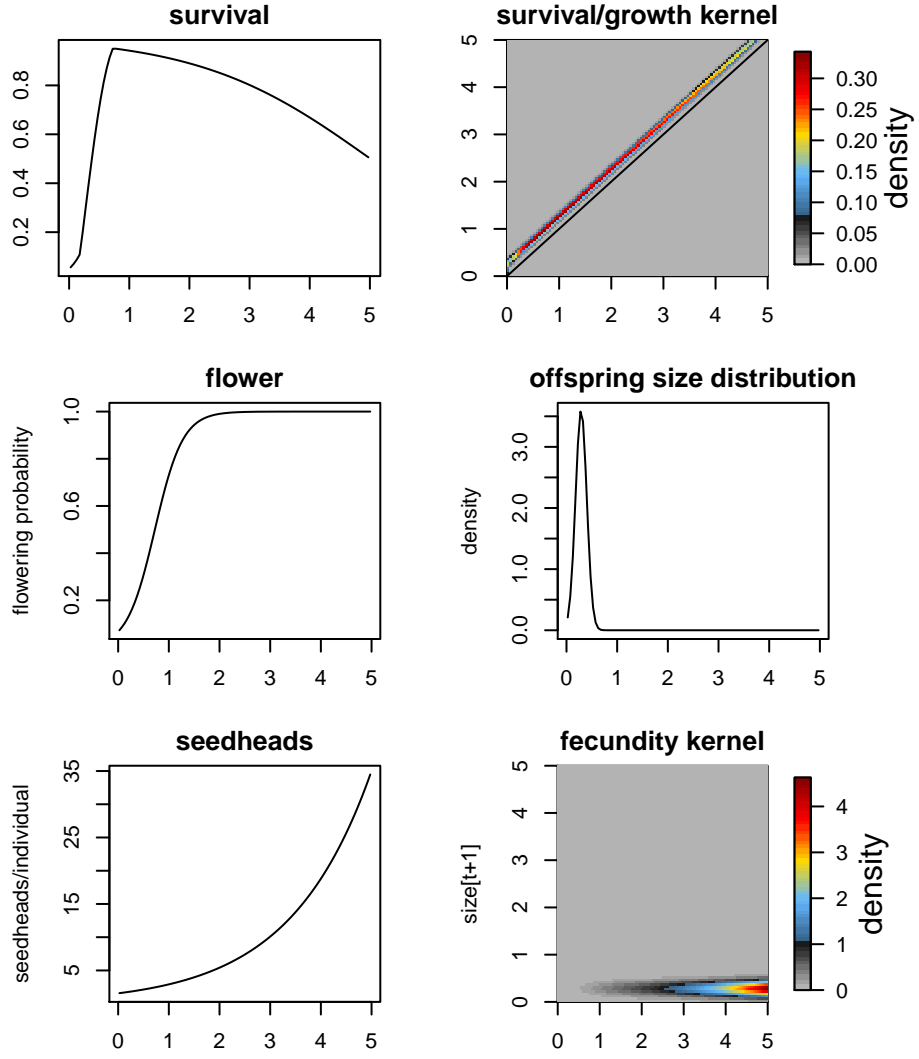


Figure A16: An example of the regressions and the kernel for a location with declining population growth ($\lambda=0.87$). Although growth is higher compared to Fig. [A15](#), the lower adult survival drives population dynamics. This is representative of the strong sensitivity parameters in the adult survival model shown in Figs. [A22](#).

7 Analyses

We can explore the predictions by comparing them using the same fire interval across the whole region (in contrast to the more realistic heterogeneous fire used in the main text). *P. repens* clearly fairs well under shorter fire return times, in part due to increasing adult mortality with size/age. Western populations are predicted to be relatively robust to different fire intervals, whereas eastern populations are best in the 12-18 year range.

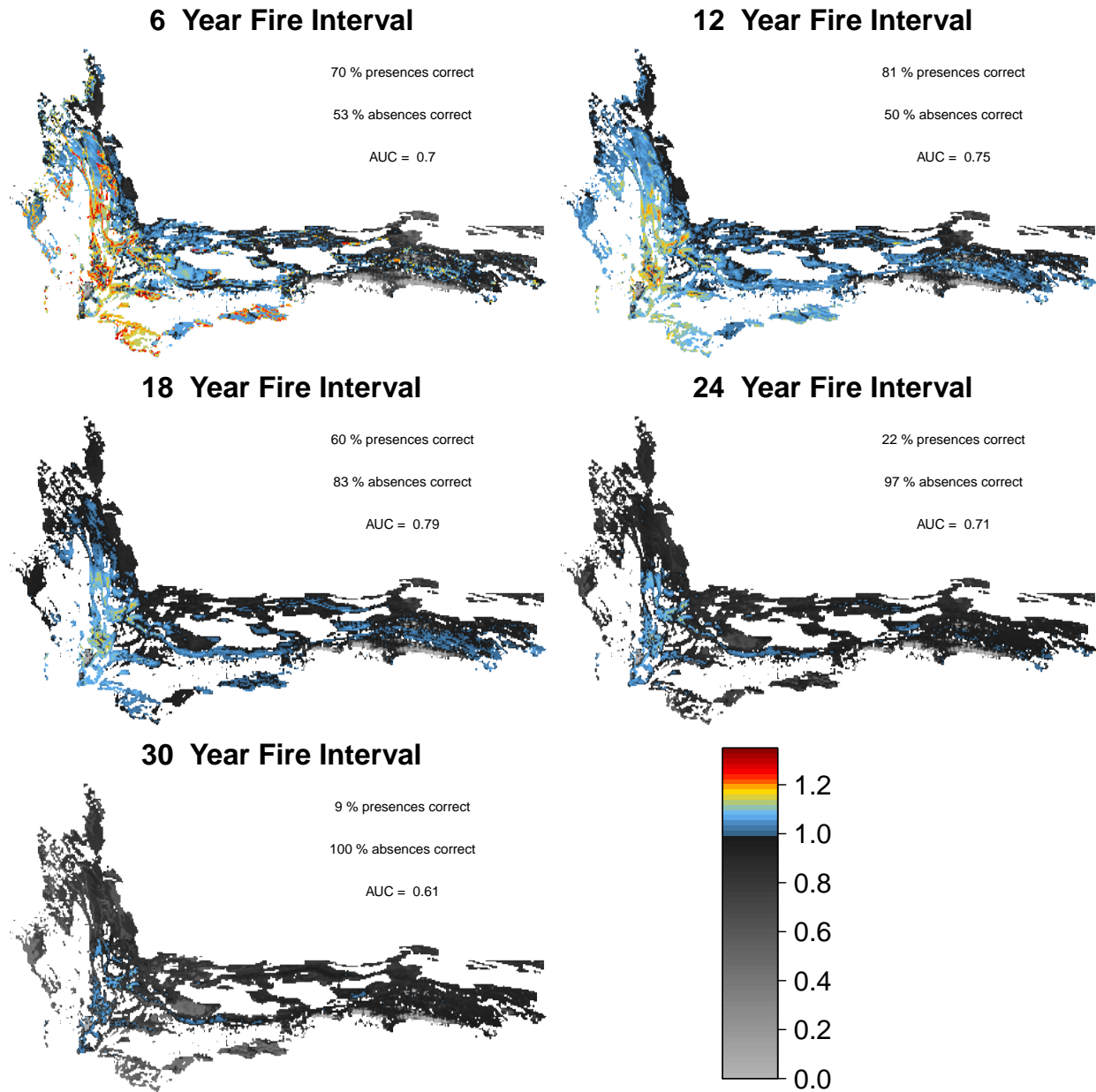


Figure A17: Common deterministic fire interval across the entire region.

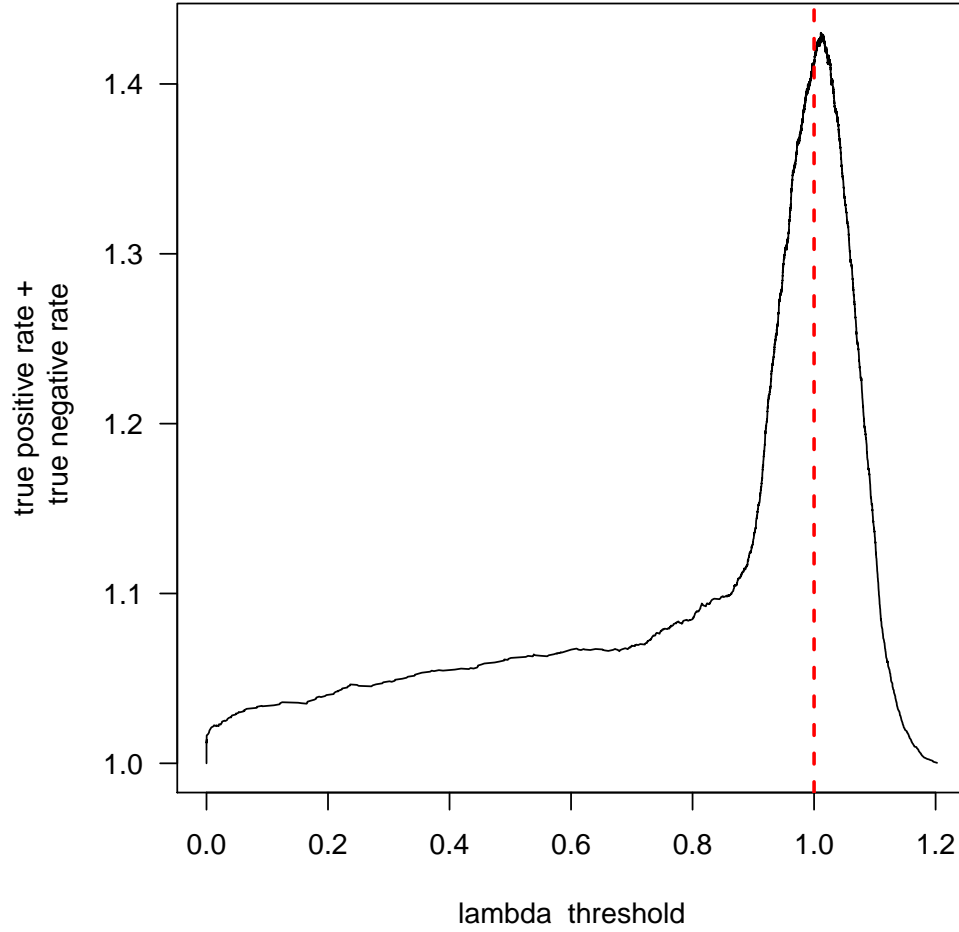


Figure A18: Exploration of potential predictive accuracy for other thresholds of λ . The accuracy, measured as the sum of the proportion of correctly presences and absences peaks near $\lambda = 1$, indicating that our DDDM is a reasonable predictor of where viable populations can persist. For example, if this peak were below, it would indicate that our models were biased toward underestimating population growth.

8 Uncertainty

The uncertainty in any population statistics can be calculated by building IPM kernels from posterior samples of the regressions. For the following analyses, we sampled regression parameters from vital rate models and calculated the population statistics to describe their uncertainty.

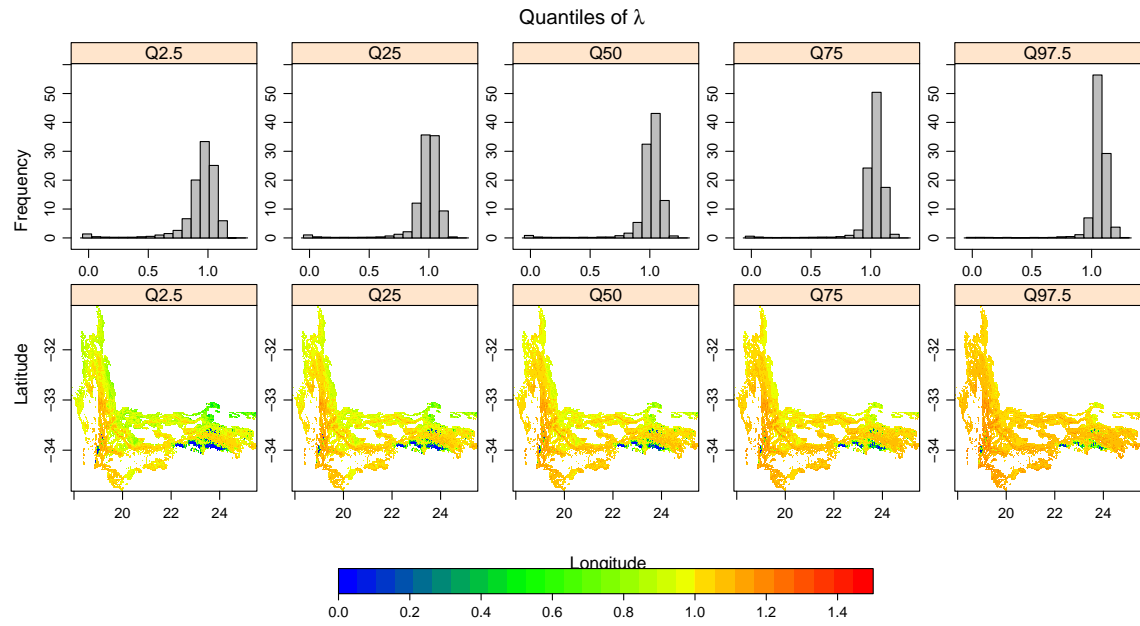


Figure A19: Illustration of the quantiles of the posterior λ distributions. The top row shows the distributions of each quantile (marginalized over space), and the bottom row shows the spatial distribution of values.

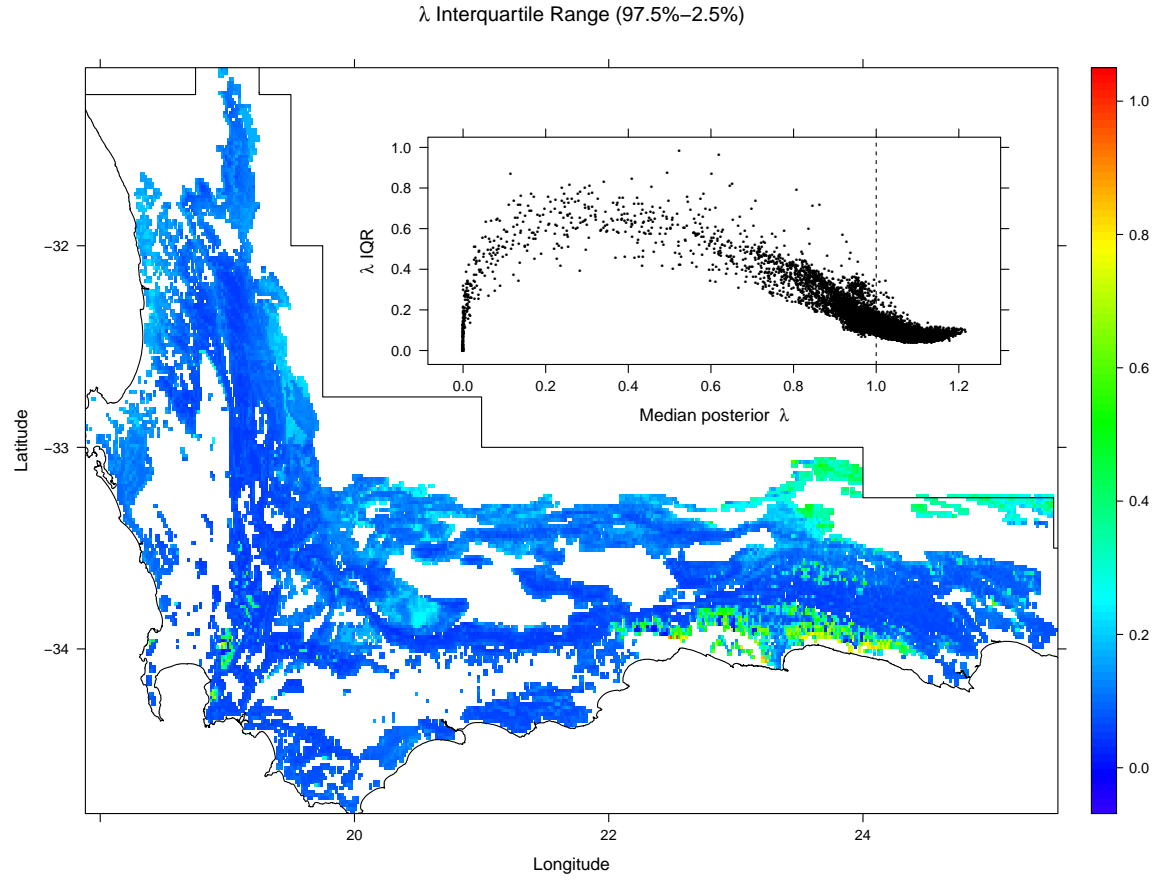


Figure A20: Interquartile range (IQR) of λ for each pixel. The inset shows the relationship of the IQR with the median posterior value of λ . Note that the uncertainty in λ is fairly low (< 0.2) for most pixels with a median value greater than 1. The pixels with the highest uncertainty (largest IQR) tend to have low-intermediate values of λ (0.1–0.6).

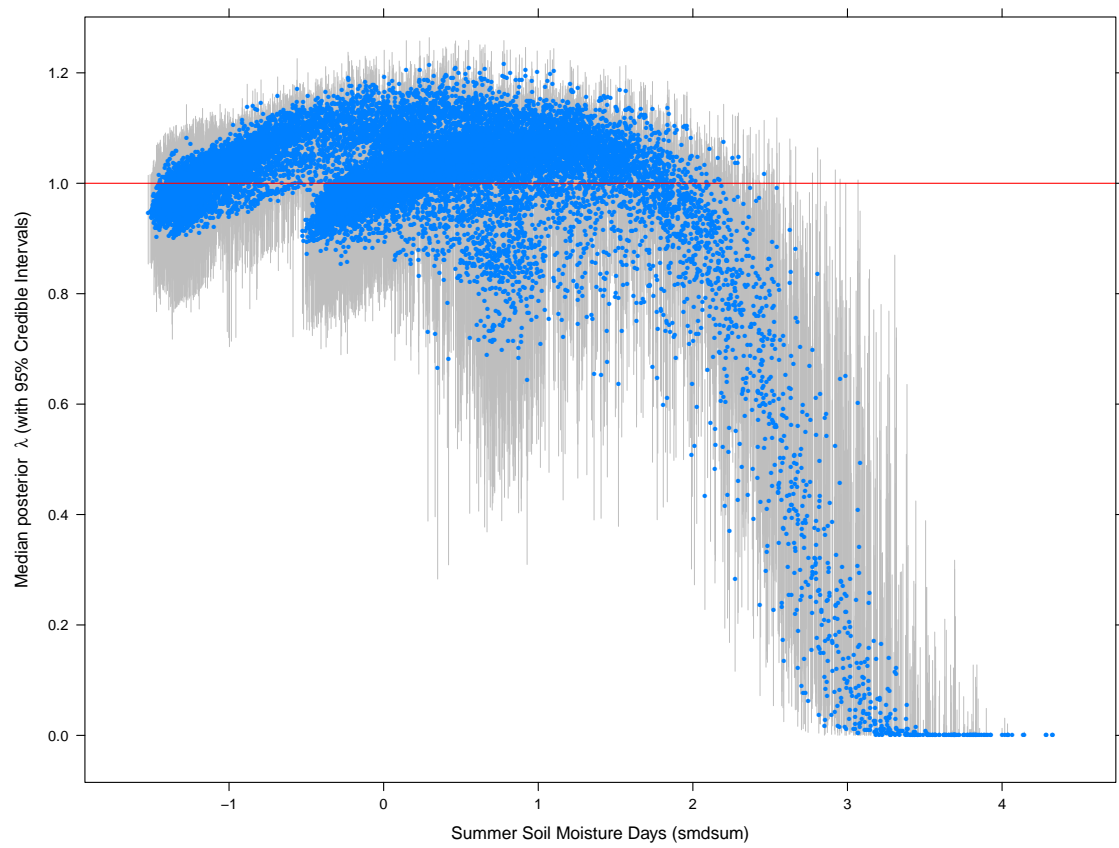


Figure A21: Relationship of λ to Summer Soil Moisture Days (smdsum) with 95% credible intervals.

9 Sensitivity/Elasticity

In this section, we report the three calculations of sensitivity and elasticity reported in the main text for both present and future fire/climate scenarios.

For parameter elasticities (Figs. [A22](#), [A23](#), [A25](#), [A26](#)) the effects of increasing each parameter value by +1% are shown below. The largest effects are seen in the southeast and southwest, both of which are regions of high winter rainfall. Notably these are regions where our model incorrectly predicts absence. The highest elasticity occurs in these regions with the quadratic terms for summer soil moisture, soil acidity and soil fertility. Each of these quadratic terms is negative, hence increasing the parameter value through perturbation dampens the step unimodal response in the model (e.g. see Fig. [A2](#)). Our prediction errors in these regions likely arise because these they require extrapolation of our models beyond the data range, and predictions are sensitive to this extrapolation.

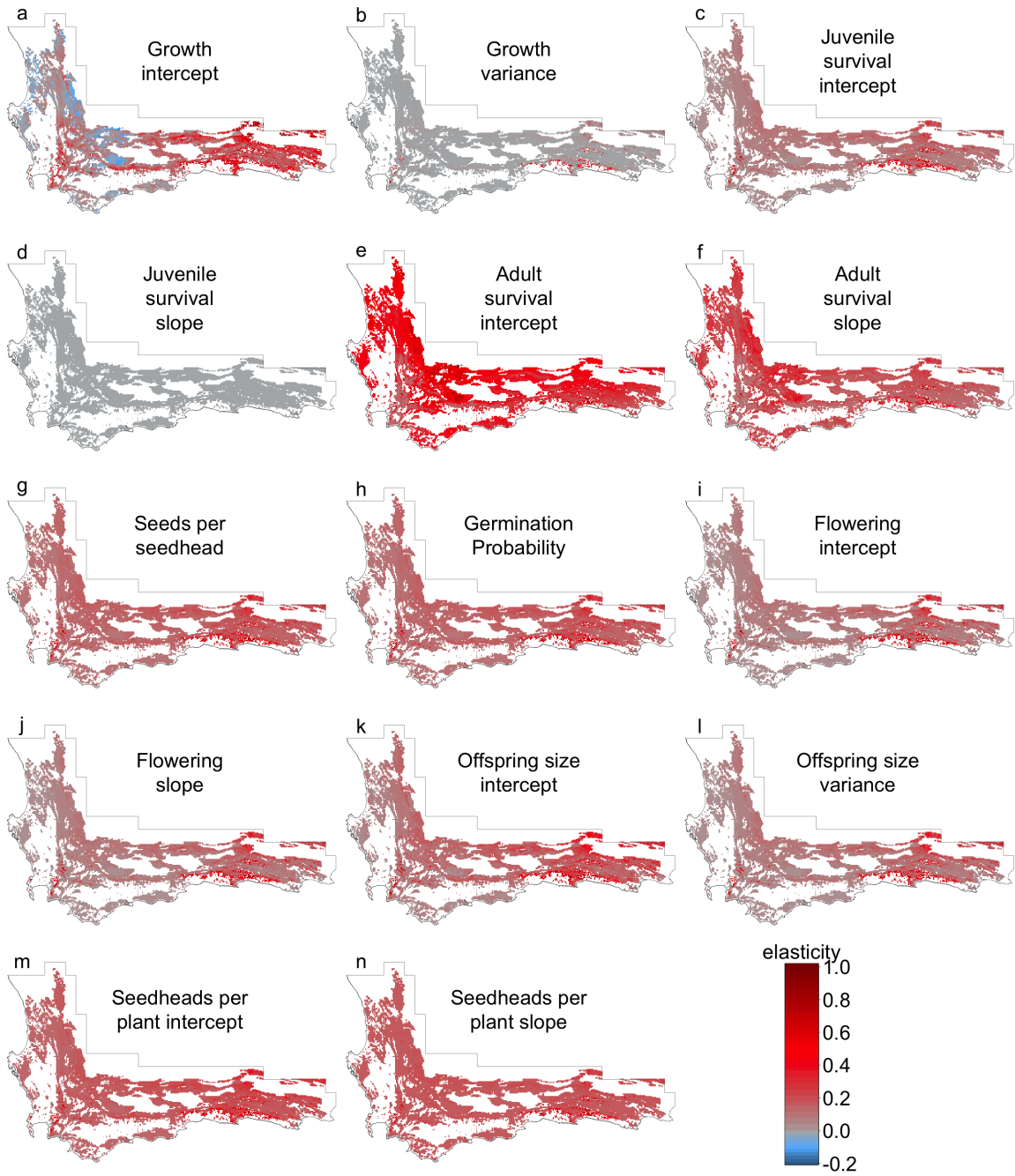


Figure A22: Elasticity to intercept and size-based regression parameters in present climate scenario. These were calculated through perturbation as $(\lambda_{perturbed} - \lambda_{true})/(\delta \lambda_{true})$ where $\delta = +0.01$. A subset of these are shown in Fig. 6 in greyscale in the main text.

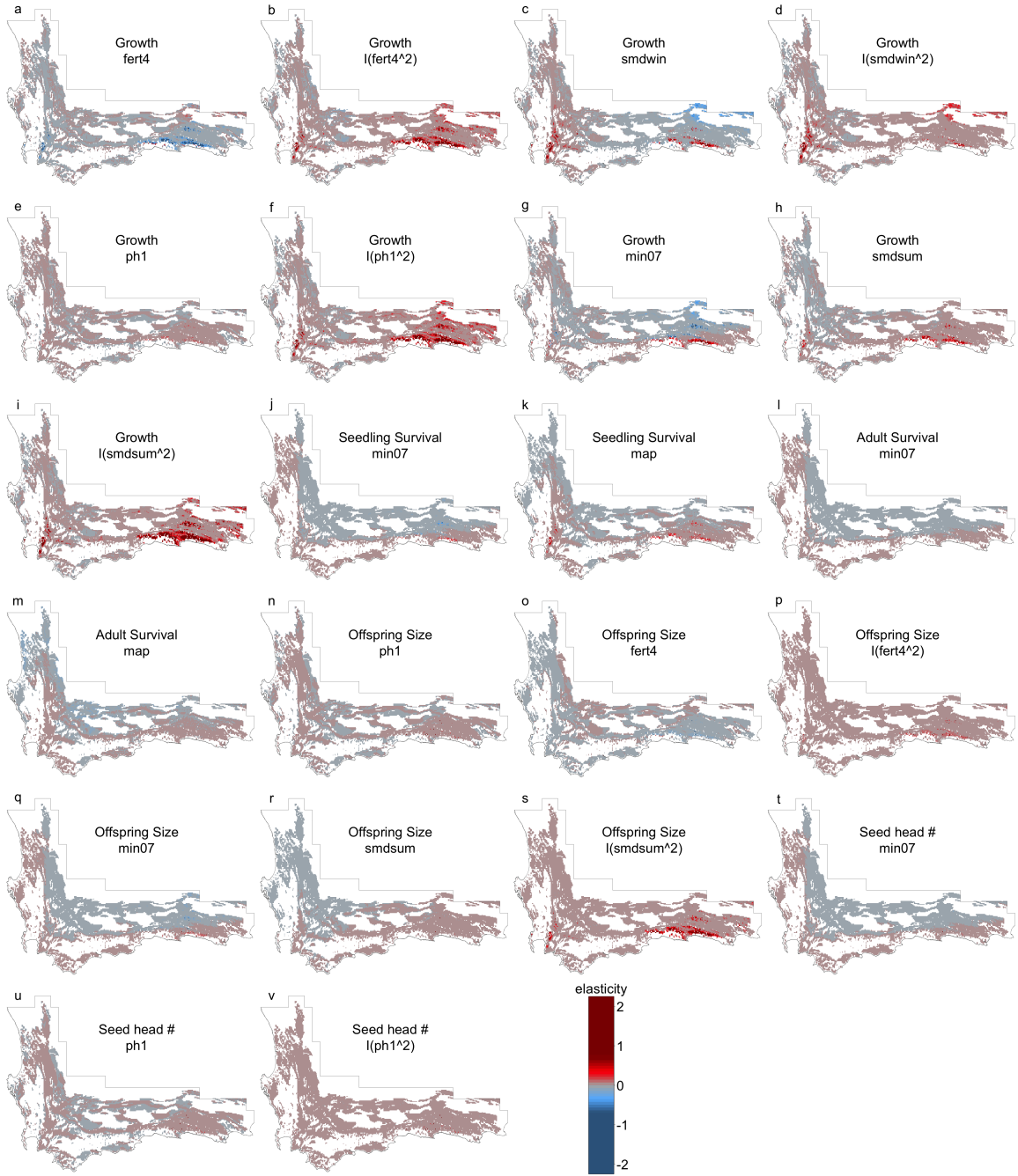


Figure A23: Elasticity to environmental regression parameters in present climate scenario. These were calculated through perturbation as $(\lambda_{perturbed} - \lambda_{true})/(\delta \lambda_{true})$ where $\delta = +0.01$.

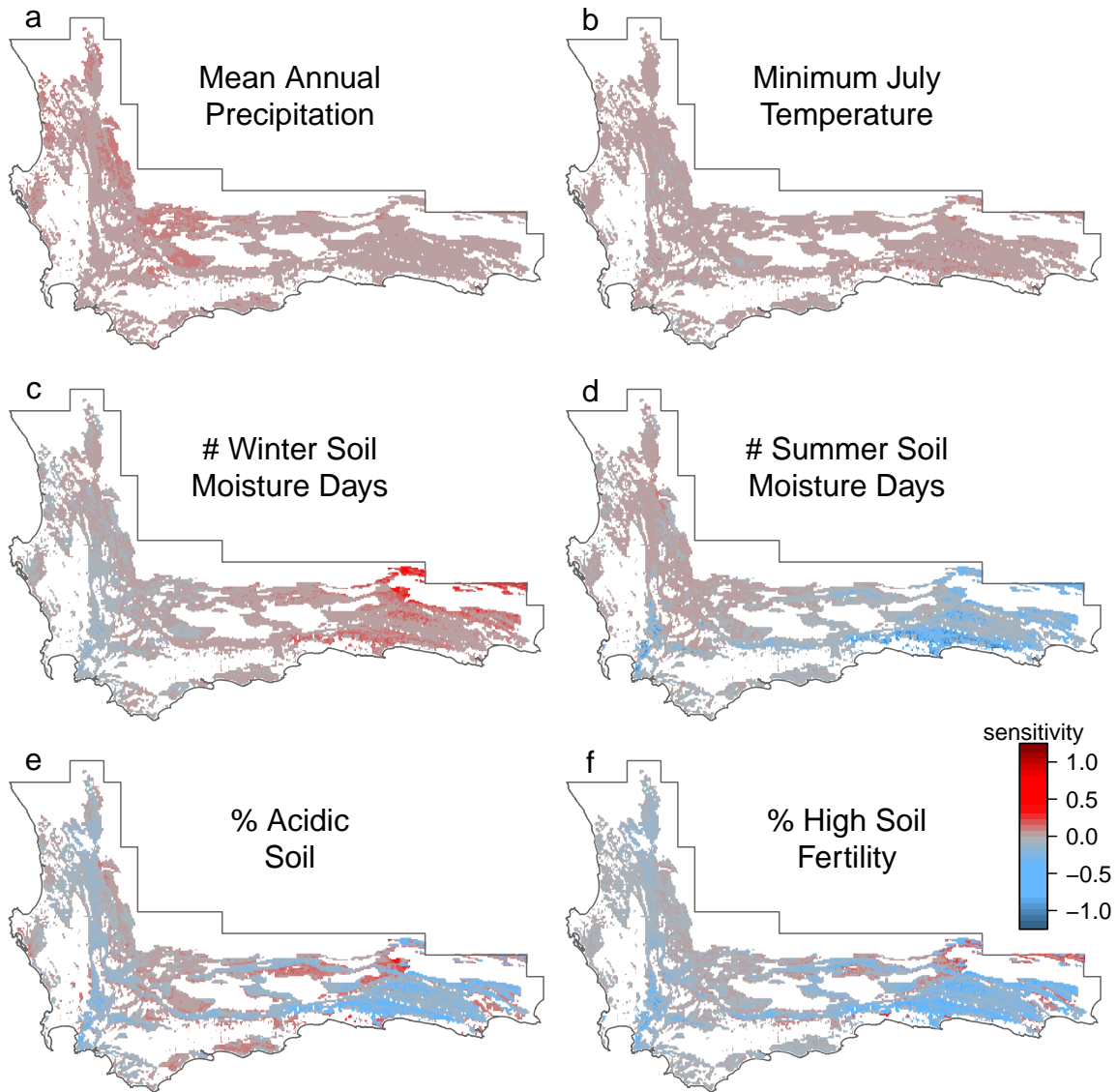


Figure A24: Sensitivity to environmental covariates in present climate scenario. This is a color reproduction of Fig. 7 in the main text to show patterns more easily. Negative responses were apparent to increases in the proportion of acidic soil or high fertility soil across the core of the predicted range. Modeled response to acidic soil is unimodal for both growth and seedhead production, hence increasing the proportion of the available landscape with acidic soil reduces population growth. Extrapolating beyond the range of the data also predicts a strong negative response of growth and offspring size (Figs. A2 and A11) to increased soil fertility (f). While in general this species is most prevalent on low-fertility soils, we think this quadratic extrapolation overstates the response of the species to prevalence of soil type.

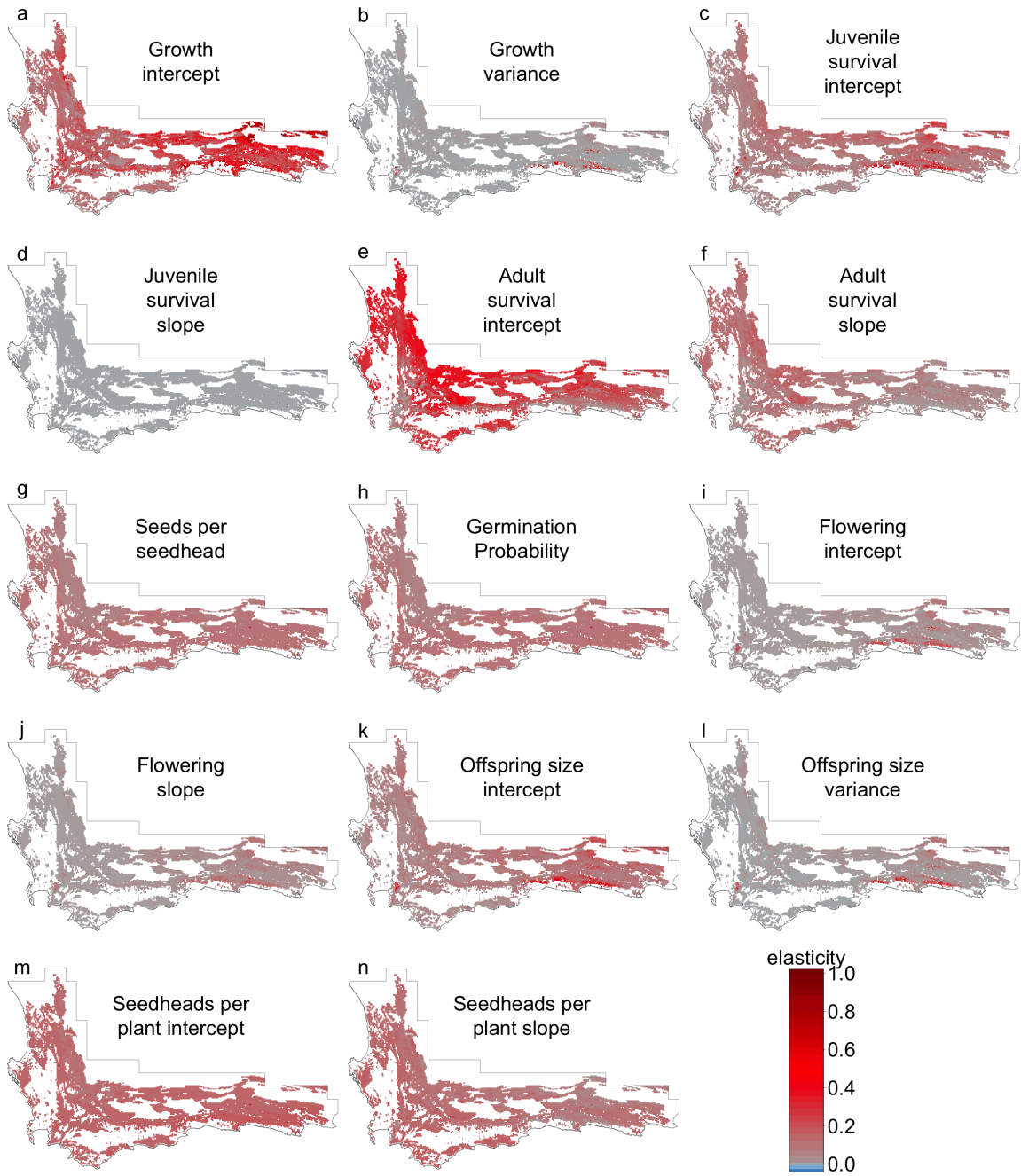


Figure A25: Elasticity to intercept and size-based regression parameters in a future climate scenario where temperatures increase by 1 degree and precipitation decreases by 10%. These were calculated through perturbation as $(\lambda_{perturbed} - \lambda_{true}) / (\delta \lambda_{true})$ where $\delta = +0.01$. A subset of these are shown in Fig. 5 in greyscale in the main text.

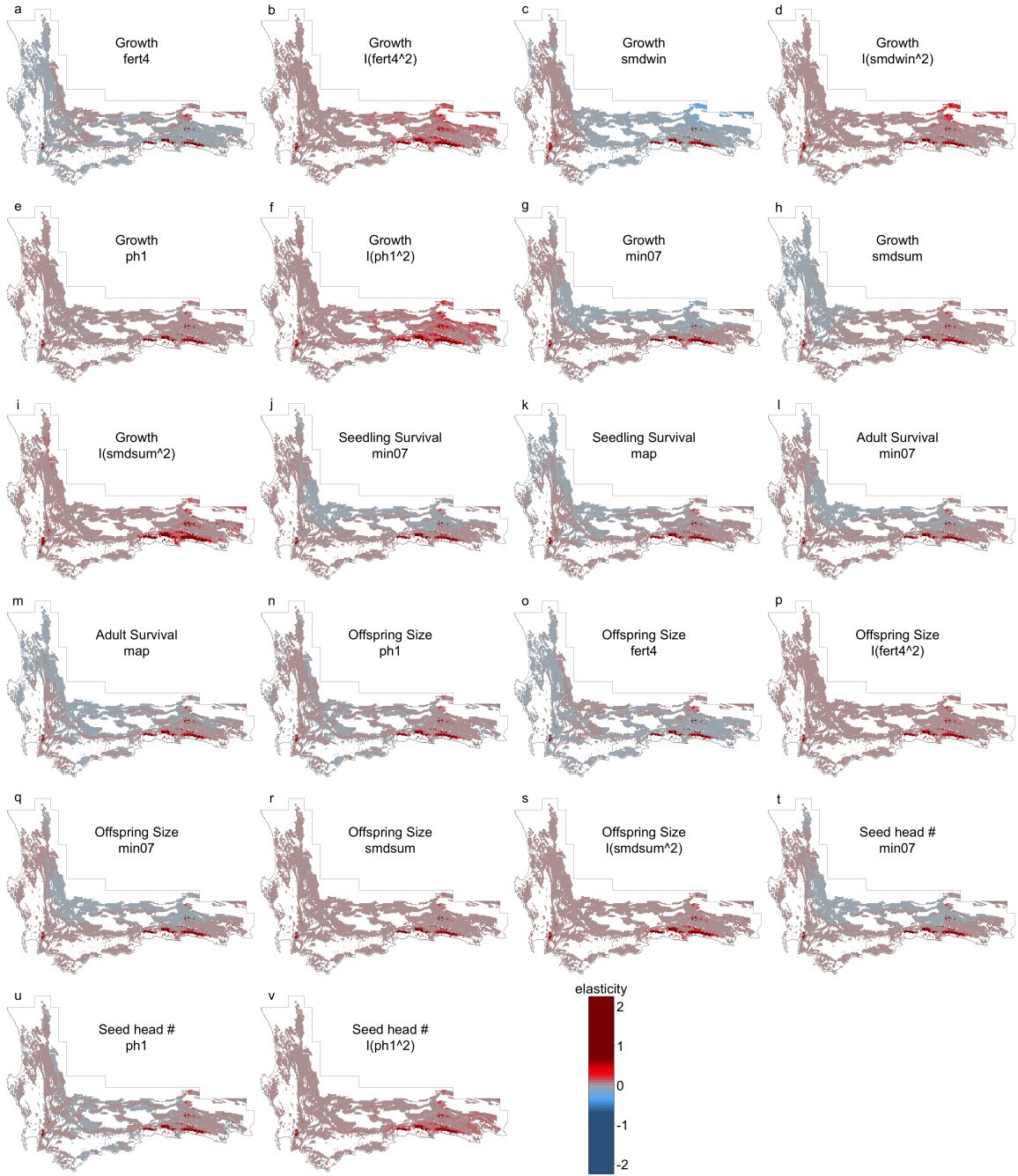


Figure A26: Elasticity to environmental regression parameters in a future climate scenario where temperatures increase by 1 degree and precipitation decreases by 10%. These were calculated through perturbation as $(\lambda_{perturbed} - \lambda_{true})/(\delta \lambda_{true})$ where $\delta = +0.01$.

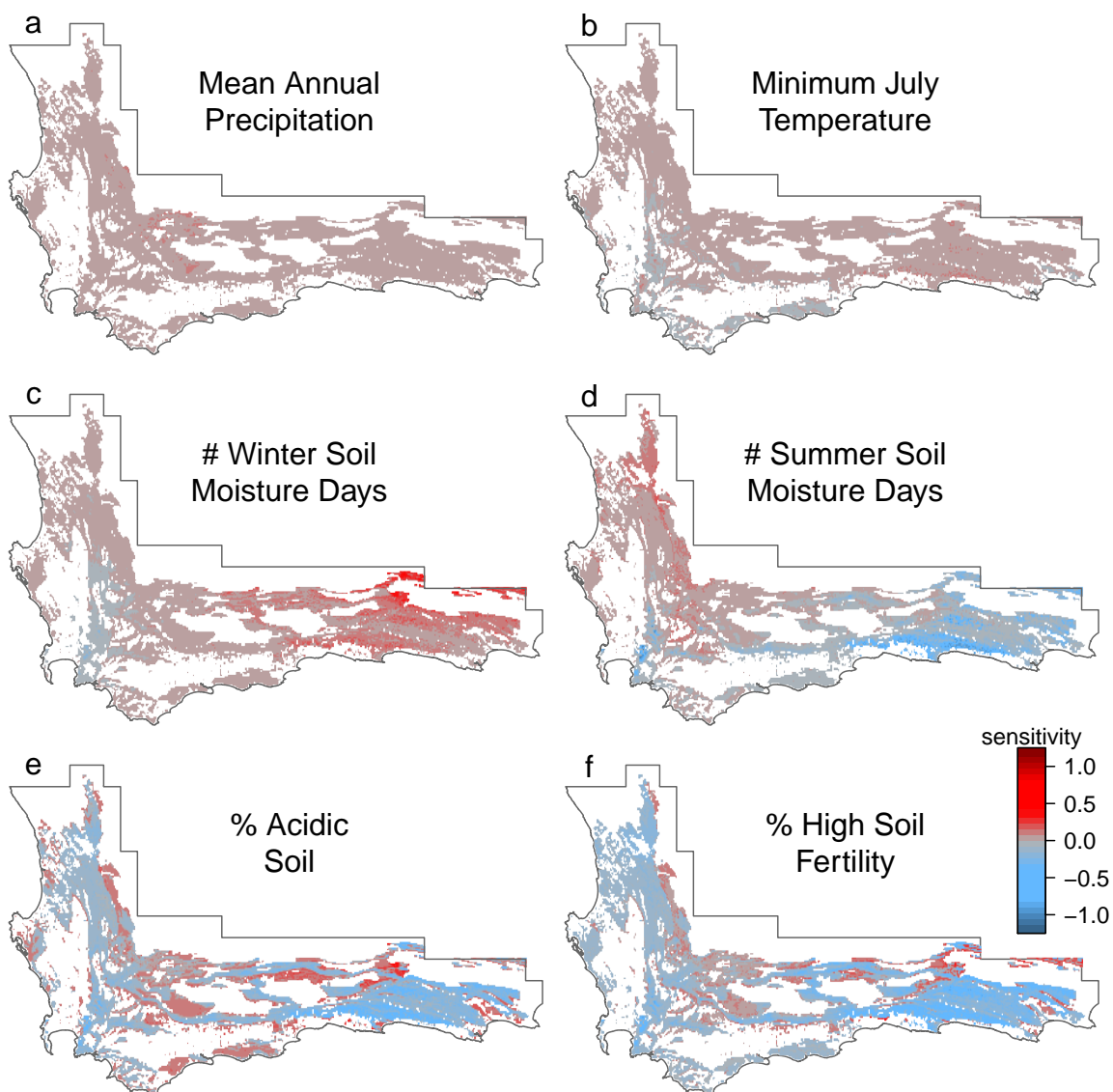


Figure A27: Sensitivity to environmental covariates in a future climate scenario where temperatures increase by 1 degree and precipitation decreases by 10%. Compare to Fig. A24), which maps the same sensitivities in the current climate scenario.

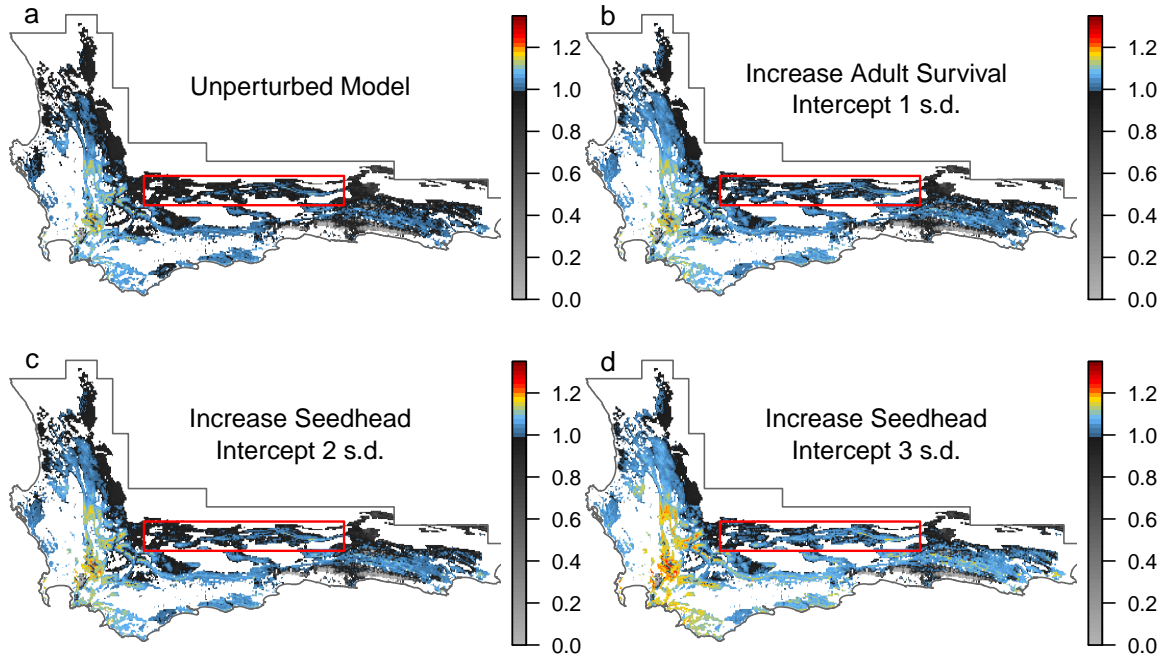


Figure A28: Results of performing 'experiments', by changing parameters to explore hypotheses. Taken together, the fecundity, survival, and population growth rate patterns suggests multiple competing hypotheses that could be evaluated with further study: (1) the fecundity data contains bias and collecting more data would show similar geographic optima to the other vital rates; (2) higher fecundity trades off with lower survival in more arid regions to sustain populations; (3) fecundity is even higher in arid regions than our model predicts, which would account for our under prediction of viable populations in this regions (Fig. 3a); (4) although the fecundity predictions are reasonable, under prediction of viable populations in arid regions occurs because adult survival is under predicted (Fig. 2b). This line of inquiry illustrates how mechanistic hypotheses can emerge from the understanding gained from DDDMs. Simulations exploring these hypotheses can further guide data collection. Hypothesis (4) appears more likely than (2) and (3) because it is only necessary to increase the intercept of adult survival by one standard deviation to improve predictions in this region, where an increase of three standard deviations in the intercept of seedhead production model is needed to achieve similar results.

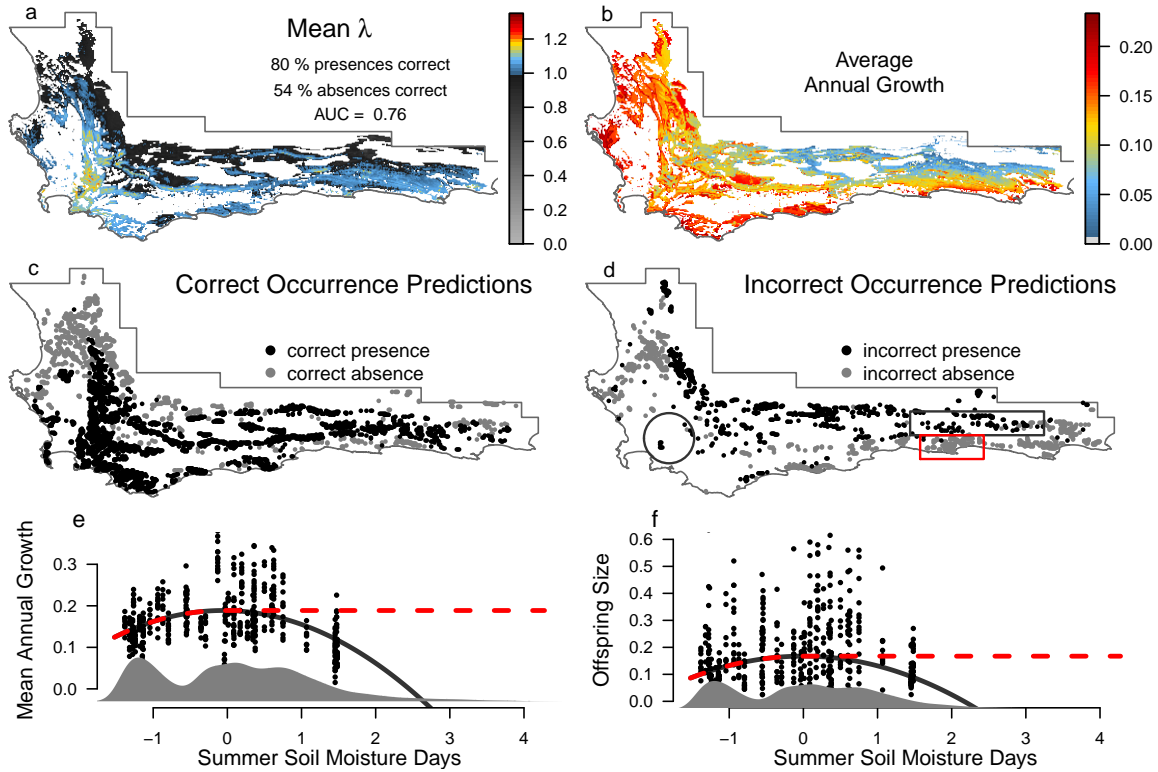


Figure A29: Results of performing 'experiments', by changing parameters to explore hypotheses. In this case, we clamped the predictions of the growth and offspring models at their maximum values along the summer SMD gradient (e,f). [Note that (e) is also shown in the main text as figure 5a.] Compare the predictions in (a,c,d) to those of the unmodified model in figure 3a,c,d in the main text. Compare the growth model predictions in (b) to figure 2c in the main text. The clamping performed here simultaneously compensates for extrapolation along the gradient for values of summer SMD > 1.5 and for two outlying populations at the high end of the gradient with slightly lower growth. This clamping reflects our expectation that *P. repens* does not perform more poorly in fynbos with more regular summer moisture. Notably, the predictions in the two high summer SMD regions (denoted by grey circle and rectangle in d). However, prediction accuracy decreases in the along the eastern coastal region (denoted by a red rectangle in d).

10 References

- Austin, M. 2007. Species distribution models and ecological theory: A critical assessment and some possible new approaches. - *Ecological Modelling* 200: 1–19.
- Spiegelhalter, D. J. et al. 2002. Bayesian measures of model complexity and fit. - *Journal of the Royal Statistical Society: Series B (Statistical Methodology)* 64: 583–639.